AMERICAN SOCIETY FOR MICROBIOLOGY | Journal of Virology

Virology | Full-Length Text

Migraine inhibitor olcegepant reduces weight loss and IL-6 release in SARS-CoV-2-infected older mice with neurological signs

Shafaqat M. Rahman,[1] David W. Buchholz,[2] Brian Imbiakha,[2] Mason C. Jager,[3] Justin Leach,[1] Raven M. Osborn,[1] Ann O. Birmingham,[1] Stephen Dewhurst,[1] Hector C. Aguilar,[2] Anne E. Luebke[1]

AUTHOR AFFILIATIONS See affiliation list on p. 12.

ABSTRACT COVID-19 can cause neurological symptoms such as fever, dizziness, and nausea. However, such neurological symptoms of SARS-CoV-2 infection have been hardly assessed in mouse models. In this study, we infected two commonly used wild-type mouse lines (C57BL/6J and 129/SvEv) and a 129S calcitonin gene-related peptide (αCGRP) null-line with mouse-adapted SARS-CoV-2 and demonstrated neurological signs including fever, dizziness, and nausea. We then evaluated whether a CGRP receptor antagonist, olcegepant, a "gepant" antagonist used in migraine treatment, could mitigate acute neuroinflammatory and neurological signs of SARS-COV-2 infection. First, we determined whether CGRP receptor antagonism provided protection from permanent weight loss in older (>18 m) C57BL/6J and 129/SvEv mice. We also observed acute fever, dizziness, and nausea in all older mice, regardless of treatment. In both wild-type mouse lines, CGRP antagonism reduced acute interleukin 6 (IL-6) levels with virtually no IL-6 release in mice lacking αCGRP. These findings suggest that migraine inhibitors such as those blocking CGRP receptor signaling protect against acute IL-6 release and subsequent inflammatory events after SARS-CoV-2 infection, which may have repercussions for related pandemic or endemic coronavirus outbreaks.

IMPORTANCE Coronavirus disease (COVID-19) can cause neurological symptoms such as fever, headache, dizziness, and nausea. However, such neurological symptoms of severe acute respiratory syndrome CoV-2 (SARS-CoV-2) infection have been hardly assessed in mouse models. In this study, we first infected two commonly used wild-type mouse lines (C57BL/6J and 129S) with mouse-adapted SARS-CoV-2 and demonstrated neurological symptoms including fever and nausea. Furthermore, we showed that the migraine treatment drug olcegepant could reduce long-term weight loss and IL-6 release associated with SARS-CoV-2 infection. These findings suggest that a migraine blocker can be protective for at least some acute SARS-CoV-2 infection signs and raise the possibility that it may also impact long-term outcomes.

KEYWORDS virus, COVID, SARS-CoV-2, viral infection, migraine, inhibitor

Coronavirus disease (COVID-19) caused by severe acute respiratory syndrome CoV-2 (SARS-CoV-2) had caused a 4-year global pandemic (1). Nausea and dizziness are early neurological symptoms of COVID-19. A 2020 study that characterized COVID-19 patients admitted to a Chicago, Illinois hospital network observed that approximately 30% of patients suffered from dizziness (2). Another multicenter cohort study in Massachusetts examined about 26% of COVID-19 patients who suffered from nausea (3), labeling this symptom as a gastrointestinal problem, but this nausea may be a function

Editor Shan-Lu Liu, The Ohio State University, Columbus, Ohio, USA

Address correspondence to Hector C. Aguilar, ha363@cornell.edu, or Anne E. Luebke, aluebke@ur.rochester.edu.

Shafaqat M. Rahman, David W. Buchholz, and Brian Imbiakha contributed equally to this article. Shafaqat M. Rahman trained Cornell personnel on motion-induced nausea/dizziness testing, contributed to experiments, and spearheaded data analyses and figure generation. David W. Buchholz and Brian Imbiakha performed all animal A-BSL3 experiments and contributed to data analyses

The authors declare no conflict of interest.

See the funding table on p. 12.

Received 10 January 2024
Accepted 15 April 2024
Published 30 May 2024

of effects from the autonomic nervous system in response to COVID-19 (4). Yet another review has noted that nausea due to COVID-19 is an early presenting symptom (5).

Therefore, it is established that nausea and dizziness are common neurological manifestations of COVID-19 infection (6–8), and in COVID-19, the severity of a patient's headache has been correlated with IL-6 levels (9). It is accepted that migraine symptoms involve the neuropeptide calcitonin gene-related peptide (CGRP). CGRP is upregulated during migraine attacks (10, 11), infusion of CGRP can induce migraine (11), and antibodies that block CGRP or its receptor can effectively treat migraine (12, 13). While CGRP has pleotropic effects on the immune system, CGRP release occurs as a result of SARS-CoV-2 activation of the transient receptor potential (TRP) channels and is implicated in COVID-19 neurological symptoms such as fever, headache, dizziness, nausea, pain, and subsequent release of interleukin 6 (IL-6) (14–16). IL-6 is an important mediator of inflammation that is often elevated in COVID-19 infection and may be involved in the hyperimmune response cascade (cytokine storm) and polarization of T cell responses (17, 18). However, there have been no studies on animal models for investigating nausea, dizziness, and fever after SARS-CoV-2 infection (19).

This research supports the testing of migraine inhibitors such as CGRP receptor antagonists, e.g., olcegepant, as a way to mitigate the neuroimmune consequences of SARS-CoV-2 infection (20).

Studies have shown that both SARS-CoV-1 and SARS-CoV-2 enter the body by binding to the angiotensin-converting enzyme 2 (ACE2) cell receptor (21, 22). However, due to sequence and structural differences between mouse ACE2 and human ACE2, human SARS coronaviruses exhibit a species-restricted tropism and are inefficient at infecting wild-type mice. To overcome this obstacle, the Baric laboratory modified two amino acids in the virus (Q498Y/P499T) to enable the virus to bind to the murine ACE2 receptor, and this modified virus (MA-10 SARS-CoV-2) was found to infect wild-type mice (23, 24). We used MA10-SARS-CoV-2 to assess both neurological symptoms of fever and dizziness/nausea in mouse models after infection. As a readout of the nausea-like state present after SARS-CoV-2 infection, we examined thermoregulatory responses to provocative motion, as we have previously used to assess migraine nausea pain (25), and others have assessed nausea in musk shrews, rats, mice, and humans (26–30). These published studies have demonstrated that provocative motion causes robust and prominent hypothermic responses, and such decreases in head temperature can represent a biomarker of a nausea-like state in laboratory animals as (i) temperature changes are only provoked by motion, (ii) differential pharmacological sensitivity of these responses mirrors sensitivity in humans, (iii) motion-induced hypothermia precedes emetic (vomiting) episodes, and (iv) there is a clear parallel in hypothermic responses between animals and humans in the underlying physiological mechanism—cutaneous vasodilatation that favors heat loss. In the nausea assay after provocative motion in mice, there is a decrease in head temperature and an increase in tail temperature. We have shown that in wild-type C57BL/6J mice, injection of CGRP prolongs the head temperature response and blunts the transient tail temperature increase, whereas a CGRP–receptor antagonist can reverse these CGRP-induced changes (31–33). Therefore, we investigated if an MA-10-SARS-CoV-2 viral infection would show similar acute nausea responses as CGRP injection, and if antagonizing CGRP signaling could reduce these nausea responses and other signs of SARS-CoV-2 infection, such as fever and weight loss.

RESULTS

MA-10 SARS-CoV-2 infection induces a fever-like state and disrupts thermoregulation to provocative motion

We measured baseline head temperatures in 18-month old male C57BL/6J, 129/SvEv, and 129 αCGRP-null groups of mice during pretesting and 3 days post-infection (dpi) with 10^5 pfu of MA-10 SARS-CoV-2 virus (Fig. 1A and B). Our results showed a higher head temperature at 3 dpi, indicating a fever in all mice, regardless of the strain and olcegepant pretreatment (Fig. 1B).

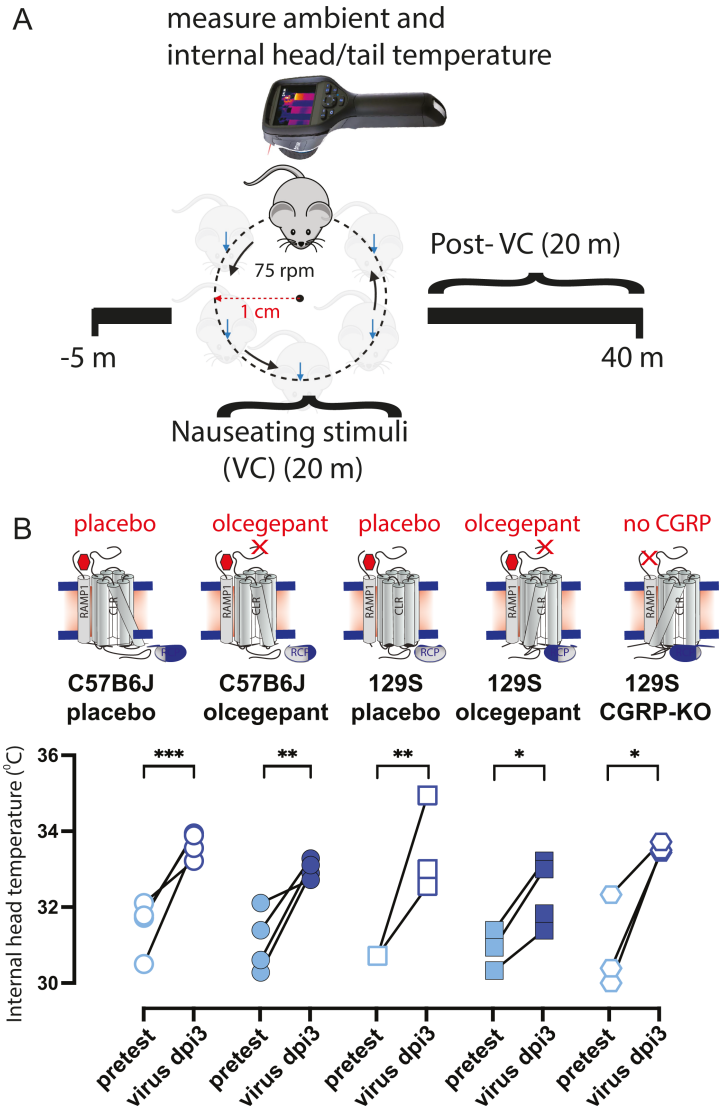

FIG 1 Eighteen-month-old C57BL/6J, 129/SvEv, and 129 mice lacking CGRP were assessed for nausea (dizziness) when subjected to an orbital rotation, noting temperature profiles (head and tail). (A) Head and tail temperatures of mice were measured for a total of 45 minutes using an FLIR E60 IR camera (model: E64501). This camera was connected to a tripod and positioned approximately 43 cm above an open, plexiglass box (mouse box) used to house an individual mouse during testing. Both the tripod and mouse box are securely attached to the shaker's base. Briefly, baseline measurements were recorded for 5 minutes prior to the provocative motion (–5 to 0 mins). The provocative motion was an orbital rotation (75 rpm, 2 cm orbital displacement), and mice were recorded for 20 minutes (0 to 20 mins). After 20 minutes, the provocative motion was turned off, and mice were recorded for an additional 20 minutes to measure recovery to baseline (20 to 40 mins). Three mouse strains were tested: C57/B6J WT, 129S WT, and 129S αCGRP-null mice. Within each wild-type (WT) strain, four groups of mice were tested: placebo only, olcegepant only, placebo with 10^5 MA-SARS-CoV-2, and olcegepant with 10^5 SARS-CoV-2 MA-10. Virus-infected mice were tested at Cornell University's A-BSL3 environment, with all preinfection testing performed at the University of Rochester. (B) All tested mice experienced a fever-like state 3 days post-viral infection (3 dpi). Olcegepant did not have a protective effect in reducing this acute fever-like state at 3 dpi. Significance is listed as *= $P < 0.05$, ** =$P < 0.01$, and ***= $P < 0.001$.

We also measured nausea readout and weight changes in 18-month old male C57BL/6J, 129/SvEv, and 129 αCGRP-null groups of mice at 3 dpi with 10^5 pfu of MA-10 SARS-CoV-2 virus (Fig. 2A). Nausea was pretested in each mouse 5–7 days prior to

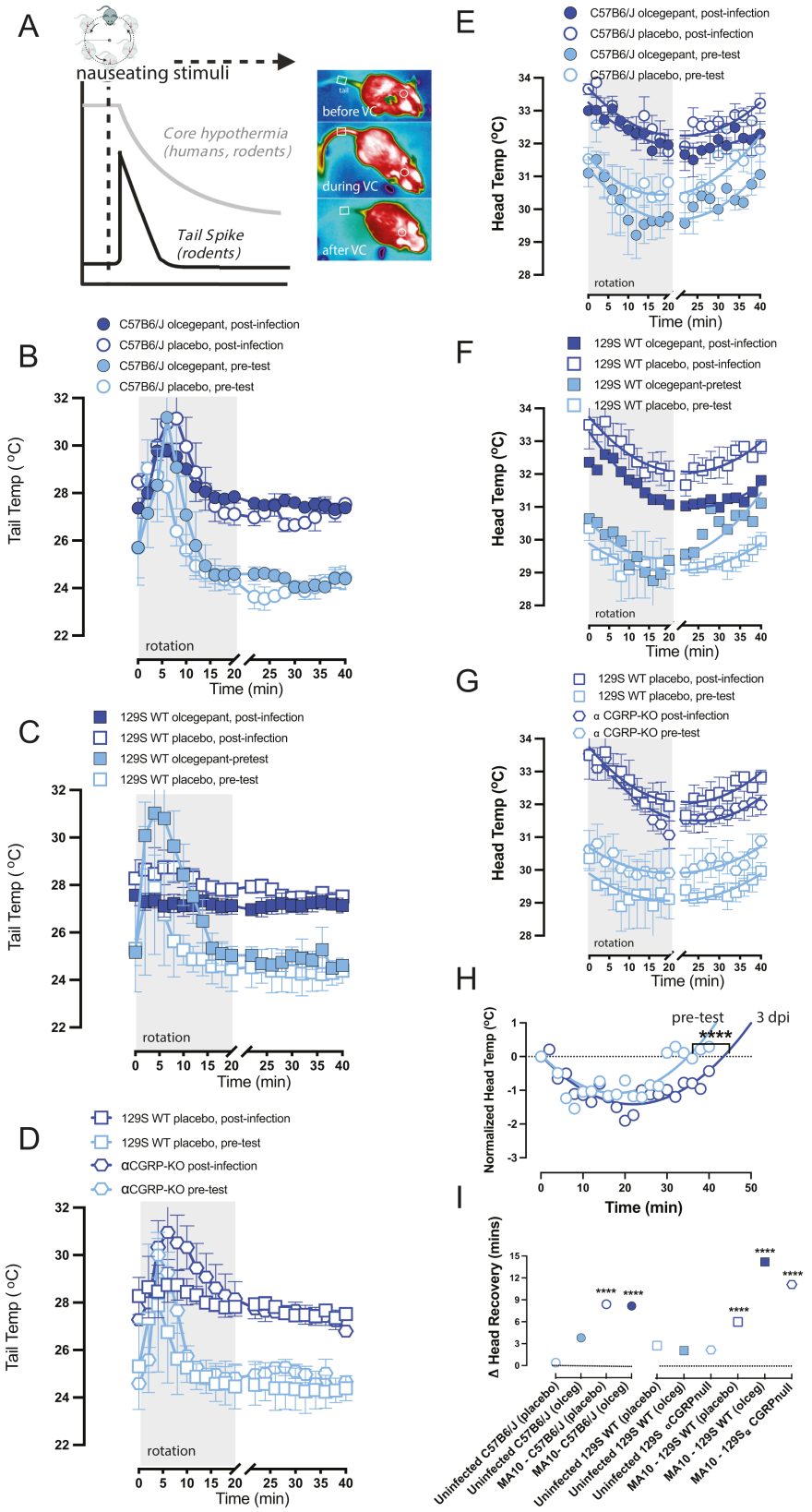

FIG 2 (A) Upon provocative motion, humans and mice will show a decrease in head temperature, which recovers once rotation is ceased, and mice show a transient tail spike ~10 minutes into rotation. Heat image examples similar to (25). When nausea or dizziness is present, the head temperature decrease

(Continued on next page)

FIG 2 (Continued)

takes longer to recover, and the transient tail spike diminishes or disappears. (B, C, D) Viral infection diminishes tail vasodilations and impairs a mouse's natural response to the provocative motion. At time t = 0, mice experience a 20-minute provocative motion and exhibit a significant increase in tail temperature. Δ tails are computed and are corrected for ambient temperature. Findings suggest that olcegepant did not protect against virus-induced changes in tail vasodilation at 3 dpi in all the strains tested. (E, F, G) Viral infection impacts recovery from hypothermia after provocative motion. (H) Second-order curve fits the observed recovery of head temperatures after provocative motion to baseline. Across all strains, infected mice experienced delayed temperature recovery compared to the pretest, with longer recovery profiles (**** =$P < 0.0001$). (I) No protective effects of olcegepant were seen in temperature recovery for any of the tested strains.

the infection. During the pre-test, we observed transient tail vasodilations in response to provocative, nauseating stimuli (Fig. 2B through D). The assay involved a 5-minute baseline recording, a 20-minute rotation period (75 rpm, 2 cm orbital displacement), and a 20-minute recovery/observation period (as shown in Fig. 2A). Tail temperature profiles also indicated a fever-like state after infection with MA-10 SARS-CoV-2, with higher tail temperatures at all timepoints during the 3 dpi test than during the pretest (Fig. 2B through D). We computed a shift in the Δ tail vasodilations by subtracting the magnitude of Δ tail vasodilations at 3 dpi from an animal's pretest Δ tail vasodilation. Apart from infected αCGRP-null mice, we observed a decrease in the magnitude of tail vasodilations in infected mice compared to their pretest, as indicated by a negative change in the Δ tail vasodilation, a sign of change in the level of severe dizziness/nausea-like state.

Typically, a 20 minute provocative rotation in mice causes observable hypothermia, and an additional 20 minute recovery period is needed for the mice to recover to their baseline head temperature. Interestingly, we observed that viral infection delayed this recovery period, as seen in our raw data (Fig. 2E through G). Using a second-order polynomial fit ($B_0 + B_1X + B_2X^2$), we estimated the time required for the mice to recover back to their baseline head temperature by interpolating a curve fit to t = 50 minutes (Fig. 2H). We then computed a Δ head recovery by subtracting the recovery period at 3 dpi from the pretest, where a positive Δ head recovery indicated a longer recovery period due to the infection. In all infected males, regardless of olcegepant treatment or strain, we observed a longer recovery period at 3 dpi ($P < 0.0001$). No protective effects by olcegepant were seen in head temperature recovery for either strain (Fig. 2H).

Olcegepant blockage or developmental loss of the CGRP receptor leads to reduced IL-6 production in response to MA-10 infection

Interestingly, SARS-CoV-2-infected 129/SvEv mice treated with olcegepant pellets had lower interleukin 6 (IL-6) concentrations in their bronchoalveolar lavage (BAL) as compared to mice treated with placebo ($P < 0.05$) (Fig. 3B). Congruently, the lower IL-6 concentrations in olcegepant-treated mice were similar to the IL-6 concentrations measured in the αCGRP-null mice (Fig. 3B), which is consistent with the relationship between CGRP and IL-6 levels in migraine (34). In C57BL/6J mice, similar trends in olcegepant effects in reducing IL-6 post-infection were observed, but they did not reach statistical significance (Fig. 3A).

Older mice treated with olcegepant recovered from the initial weight loss by 7 dpi

When 18-month old C57 or 129S wild-type mice were infected with MA-10, those pretreated with olcegepant pellets showed a faster recovery to baseline weight compared to mice that received placebo pellets. This effect was observed in both female and male C57BL/6 J mice (Fig. 4A), as well as in older female and male 129/SvEv mice (Fig. 4B). Notably, αCGRP-null mice of either sex experienced similar trends as olcegepant-administered 129S WT mice (Fig. 4E). Furthermore, older infected mice exhibited

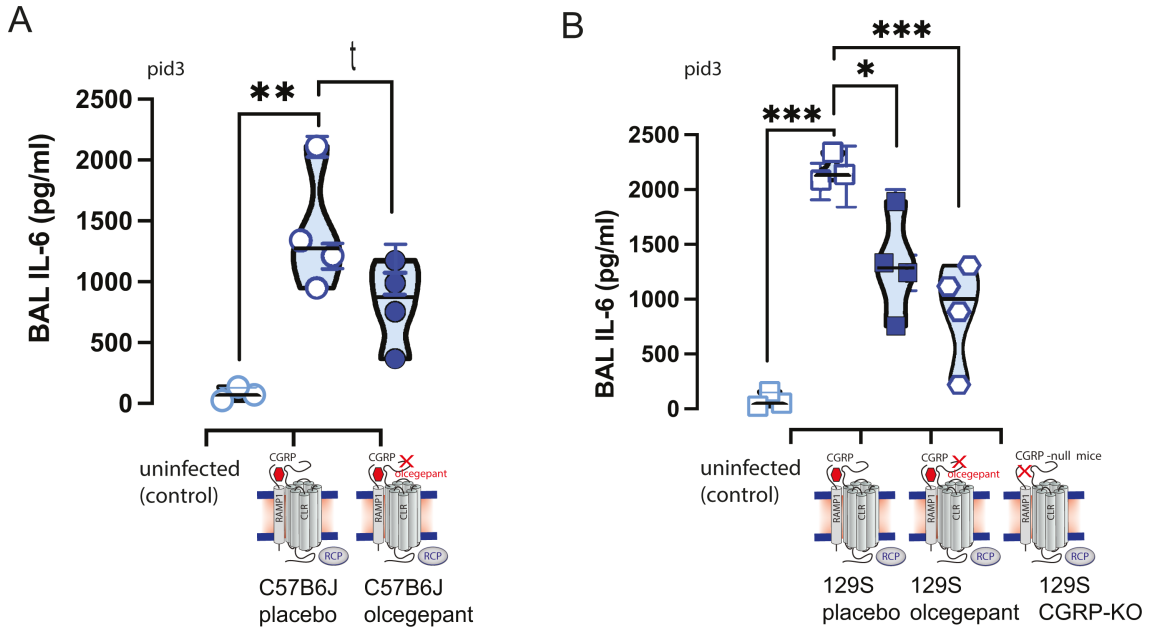

FIG 3 Bronchoalveolar lavage (BAL) samples were obtained for ELISA testing, and lungs were obtained for subsequent immunohistochemistry at 3 dpi and were analyzed with nested 1-way ANOVA. MA10-SARS-CoV-2 infection increased the release of the inflammatory cytokine IL-6, and this IL-6 release was attenuated by the CGRP signaling blockade. In both C57BL/6J (A) and 129S (B) mouse strains, IL-6 release was attenuated by olcegepant SQ release. Moreover, in αCGRP-null mice (αCGRP-KO), IL-6 cytokine release was statistically equivalent to infected controls given olcegepant and uninfected controls. Significance is listed as *= $P < 0.05$, ** =$P < 0.01$, and ***= $P < 0.001$, and the italicized *t* represents *P*-value < 0.1.

lower core temperatures compared to the uninfected groups. However, olcegepant had no distinguishable effect on core temperatures regardless of age or strain (Fig. 4B, D and F). In addition, MA-10 infection did not significantly impact O_2% saturation levels in mice regardless of age, sex, or strain. However, αCGRP-null mice exhibited lower weight loss trends following virus infection than WT mice, suggesting that the αCGRP-null mice had reduced signs of disease.

Histological analysis of lung tissue revealed no significant differences in the number of SARS-CoV-2 infected cells in the lungs of C57BL/6J or 129S WT mice at 3 dpi (Fig. 5A and B). However, olcegepant-treated mice and αCGRP-null mice showed reduced staining for SARS-CoV-2 when compared to placebo-treated mice, and this observation correlated with the reduced IL-6 levels. Figure 5C and D shows SARS-CoV-2 staining (scale = 100 µm) of C57BL/6J (C) and 129S (D) lung tissues.

DISCUSSION

Neurological symptoms of SARS-CoV-2 infection have been hardly assessed in mouse models. Here, we infected two commonly used wildtype mice lines (C57BL/6 and 129S) with mouse adapted SARS-CoV-2 strain MA-10. Importantly, we demonstrated for the first time the neurological symptoms such as fever and dizziness/nausea-like state elicited by SARS-CoV-2 MA-10 at 3 dpi. These results are consistent with associated fever and nausea symptoms observed in COVID patients (35, 36). Early on in the pandemic, there was a controversy as to whether CGRP plasma levels were increased or decreased in COVID-19 disease (37, 38). However, a recent study with a relatively higher number of patients showed that elevated CGRP plasma levels are correlated with increased disease severity in hospitalized COVID-19 patients (39). Notably, in our study, olcegepant (small-molecule CGRP receptor antagonist) reduced weight loss post-infection as well as IL-6 release at 3 days post-infection (3 dpi) in two distinct wild-type mouse strains (C57BL/6J and 129/SvEv), even in the absence of an effect on acute nausea readouts in the infected animals.

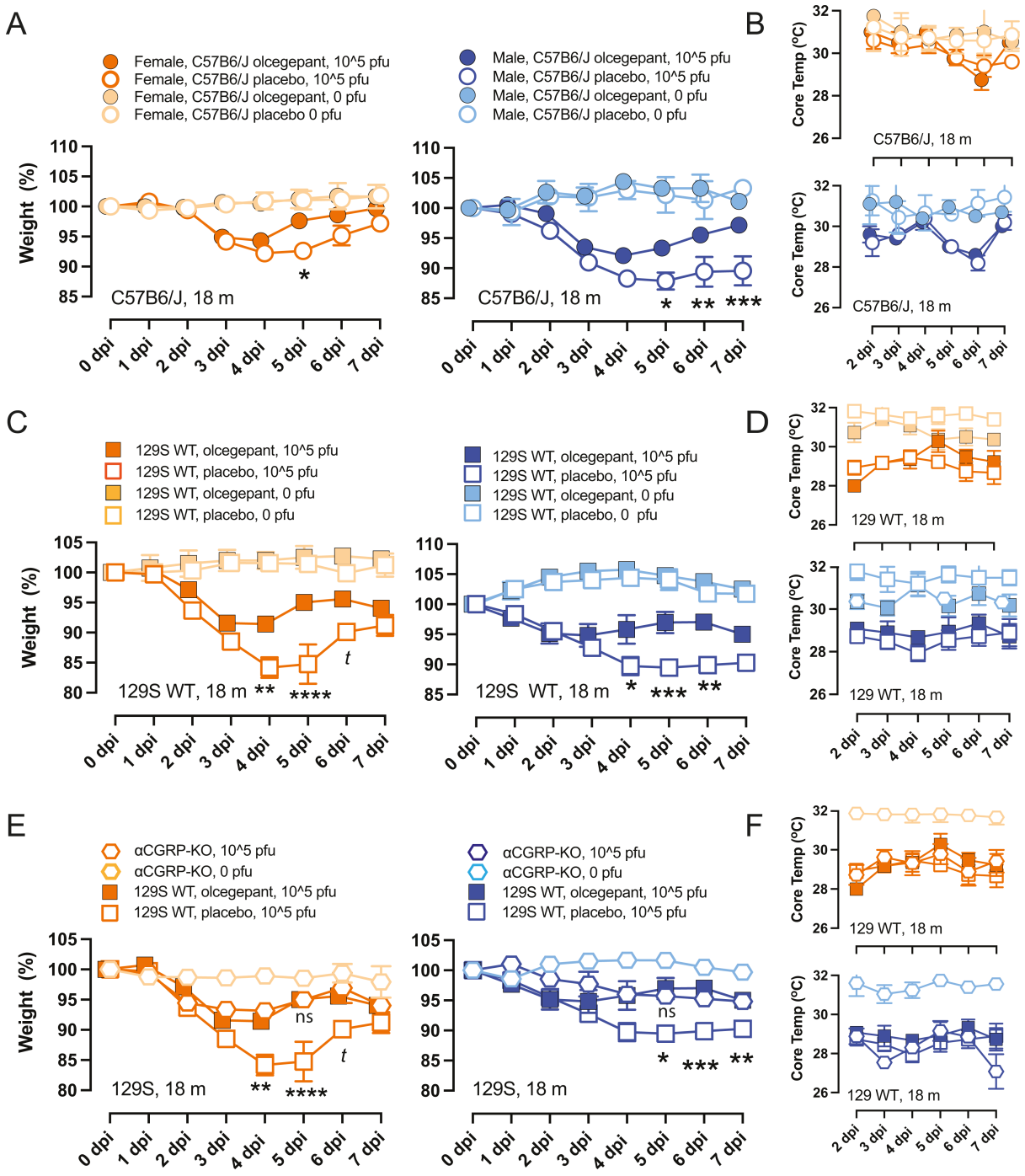

FIG 4 Older (18-month old) female and male mice were tested for weight loss and core temperature decreases after infection with MA-10 SARS-CoV-2, 10^5 pfu virus at 0–7 dpi using two-way mixed-effects models and Bonferroni multiple comparisons test. At each dpi, asterisks correspond to comparisons between placebos versus olcegepant in infected mice since no differences were observed due to olcegepant in uninfected controls (A and C) We found that animals treated with olcegepant recovered from the initial weight loss, with male mice showing increased protection. (A) C57BL/6J; (C) 129/SvEv. (E) Like the IL-6 findings (Fig. 3), mice lacking the CGRP peptide (αCGRP-KO) were not significantly different from uninfected controls. (B, D, F) Viral infection caused detected core temperatures of mice to decrease, and this effect was unaltered by olcegepant treatment. *P*-values: *= $P < 0.05$, ** =$P < 0.01$, and ***= $P < 0.001$, and *t* represents a comparison with *P*-value < 0.1.

Neuropathological changes in Parkinson's and Alzheimer's are correlated with increased IL-6 expression in the central nervous system (40), and SARS-CoV-2-infected patients with acute neurological symptoms have elevated levels of IL-6 (41). Moreover,

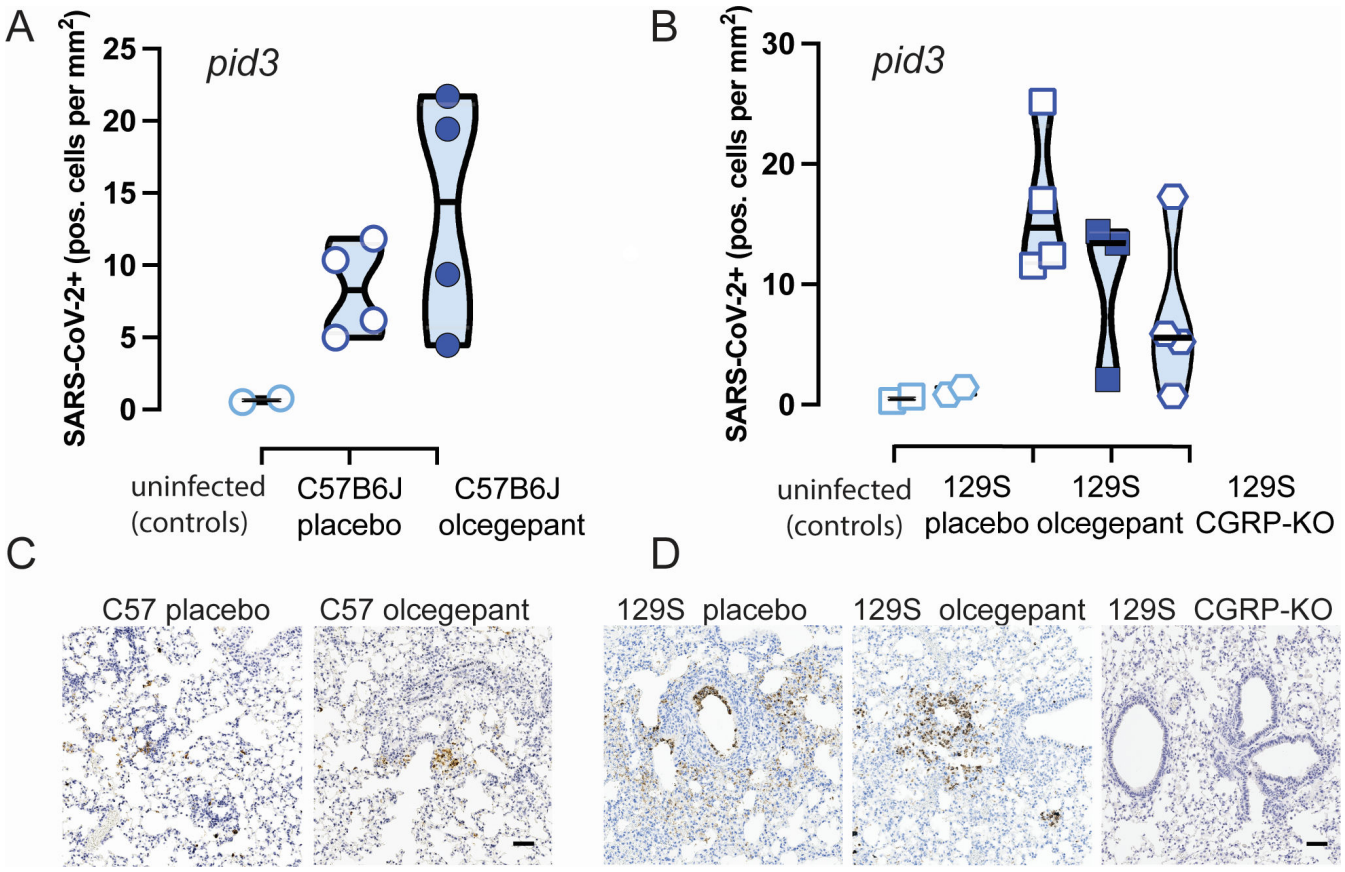

FIG 5 (A and B) There was no statistically significant difference in the number of SARS-CoV-2 antigen-positive cells in the lungs of (A and C) C57BL/6J or (B and D) 129S mice, between mice that received placebo versus olcegepant pellets at 3 dpi. (C and D) Representative SARS-CoV-2 immunostaining is shown for 3 dpi lung issues from C57B6/J (C) and 129S (D) mice. The scale bar is 100 µm.

there is a clear association between CGRP levels and IL-6 cytokines during migraine attacks (34) Interestingly, we observed IL-6 level changes (3 dpi) before we observed any behavioral effects (i.e., no differences in nausea at 3 dpi), yet differences in weight loss were observed in mice treated with olcegepant by 5 dpi. Based on this finding, we presume that like weight loss, nausea might abate sooner in animals treated with olcegepant, yet this is speculation. Several other groups have attempted to decipher the relationship between COVID-19 and IL-6. Autopsies of COVID-19 patients indicate a high infiltration of macrophages into the lungs, which significantly produce IL-6 in response to infections (42). CGRP is known to increase IL-6 mRNA expression (43), and the inverse relationship is also of importance as IL-6 augments the release of CGRP from cultured neurons (44). Thus, CGRP may induce IL-6 release, which is attenuated with olcegepant as we observed in our study, or IL-6 release from macrophages as part of the innate and adaptive immune responses may signal CGRP release from the nervous system. The current evidence suggests an intricate relationship between CGRP and IL-6 in neurological disease, but future experiments are required to determine a causative role between these factors.

While upon SARS-CoV-2 infection both the 129/SvEv and C57BL/6 mouse lines released IL-6, the 129SvEv mice were more responsive to CGRP receptor antagonism. The 129/SvEv mice have been repeatedly characterized as more sensitive to neuropathic pain than C57BL/6 J mice (45, 46), and IL-6 is a critical factor in neuropathic pain caused by peripheral nerve injury, chemotherapy-induced neuropathy, and spinal cord injury (47). Together, this suggests that MA-10 SARS-CoV-2 infection in the 129/SvEv mice may

elicit a neuropathic pain response that induces higher IL-6 release compared to C57BL/6J, as we observed in our study.

A few studies have investigated CGRP antagonism on individuals infected with SARS-CoV-2, and one study focused on testing if there was a deleterious effect on COVID-19 infections (48), which they did not find, but this study did not stratify patients by age or length of migraine treatment, which might be needed to control for differences in CGRP release. Two other case studies showed that increased headaches after SARS-CoV-2 infection can be treated with CGRP monoclonal antibodies (49, 50), presumably by reducing increased CGRP signaling after SARS-CoV-2 infection. As there are monoclonal antibodies to CGRP and to the receptor, as well as "gepants" antagonizing the receptor, it is not known if there are differences in monoclonal antibody migraine treatments versus "gepant" treatments. Because there are CGRP monoclonal antibodies that are efficacious in mouse light-aversion studies (51–55), future studies are aimed to test if there are differences in CGRP monoclonal antibody versus "gepant" treatments in SARS-CoV-2 neurological symptoms and IL-6 release.

Our study is the first to show that inhibiting CGRP signaling—via olcegepant or in the αCGRP-null mice—protects against weight loss and reduces IL-6 release in older mice. COVID-19 symptoms are more severe and mortality rates are higher in aged human patients, adding significance to our results. Our study suggests that olcegepant or other CGRP targeting treatments may be further explored particularly to treat headaches or migraine in aged individuals and/or those with high IL-6 levels upon COVID-19 infection.

In conclusion, in addition to the acute neurological effects studied here, antagonizing CGRP signaling may be an off-the-shelf therapeutic against long COVID, since long COVID patients also show higher IL-6 plasma levels (56). Long COVID has been demonstrated in mouse models (57), and future plans include investigating if antagonizing CGRP signaling in preclinical models can mitigate associated neurological symptoms of long COVID (58), as well as testing various drug dose regimens. Furthermore, the results of our study may have implications for other coronaviral diseases, such as those caused by future pandemic (SARS-CoV-1, MERS-CoV, etc.…) or endemic coronaviruses.

MATERIALS AND METHODS

Animals

A total of 180 mice aged ≥18 months (120 M/60F) were used in these studies, either 129/SvEv (Taconic 129SVE) or C57BL/6J (JAX 0664) or αCGRP (-/-) null mice on a 129SvEv background. Prior to SARS-CoV-2 infection, mice were bred and housed under a 12-hour day/night cycle at the University of Rochester 's Vivarium under the care of the University of Rochester's Veterinary Services personnel. Mice were implanted with transponder chips (Backagin Microchip FDX-B ISO 11784/11785) to allow for blinded identification and, when relevant, implanted with slow-releasing pellets containing placebo or olcegepant (BIBN4096, Tocris; 2 mg/kg/day/SQ; Innovative Research of America, Inc.). Mice were implanted with pellets and transponders 2 days (−2dpi) before SARS-CoV-2 infection. After pretesting and pellet/transponder implantation, mice were transferred to Cornell's animal biosafety level 3 (A-BSL3) facility and acclimatized 2 days prior to virus infection and testing.

Virus propagation

Vero-E6 cells (obtained through BEI resources, NIAID, NIH, and NR-53726) were cultured in Eagle's minimum essential medium (ATCC, #30–2003) supplemented with 10% (vol/vol) fetal bovine serum (FBS) (Gibco, CA) and 1% penicillin–streptomycin (Pen–Strep, Life Technologies) at 37°C in a 5% (vol/vol) CO_2 atmosphere. Viral stocks of mouse-adapted SARS-CoV-2 (MA10) (obtained from the laboratory Dr. Ralph Baric) were propagated in Vero-E6 cells in 2% (vol/vol) FBS and 1% penicillin–streptomycin at 37°C at a multiplicity of infection (MOI) of 0.1. Viral stock titers were determined by $TCID_{50}$ analysis. Viral

propagation involving live SARS-CoV-2 was conducted in biosafety level 3 (BSL3) facilities both at the University of Rochester and at Cornell University.

A-BSL3 facility and viral inoculations

Mice were anesthetized using isofluorane and subsequently intranasally infected with MA-10 SARS-CoV-2. For infection with live virus, drops of the precharacterized viral stock were administered into the rostral meatus of the nose, with a total volume of 50 µL per mouse. Daily monitoring and weighing of the mice were conducted until they reached a predetermined humane endpoint of 20% wt loss from their starting weight and/or severe clinical signs, at which point animals were humanely euthanized.

Nausea testing with thermoregulation

We studied a thermoregulation correlate of nausea, previously published as a robust, surrogate behavior in rats, musk shrews, mice, and humans (25–30, 59, 60). Head and tail temperatures of C57B6/J mice were measured for a total of 45 minutes by using a FLIR E60 IR camera (model: E64501). This camera was connected to a tripod and positioned ~43 cm above an open, plexiglass box (mouse box) used to house an individual mouse during testing. Both the tripod and mouse box were securely attached to the shaker's base. Briefly, baseline measurements were recorded for 5 minutes prior to the provocative motion (–5 to 0 mins). The provocative motion was an orbital rotation (75 rpm, 2 cm orbital displacement), and mice were video-recorded for 20 minutes (0 to 20 mins). After 20 minutes, the provocative motion was turned off, and mice were video-recorded for an additional 20 minutes to measure recovery to baseline (20 to 40 mins). Head and tail temperatures were measured after data retrieval using the software FLIR Tools+. Tail and head temperatures were measured within the predefined field of views: the square region (3 × 3 mm) for the tail and the circular region (10 × 10 mm) for the head, as shown in Fig. 2A and previously described in (25). Tail measurements were conducted 2 cm from the base of the tail and head measurements at the center of the head image, in between the mouse's ears. Infrared imaging data were collected every minute during baseline measurements and every 2 minutes during and after the provocative motion. We quantified thermoregulatory changes to provocative motion by comparing changes in tail vasodilatations, and we approximated the magnitude of the head hypothermia based on second-order curve fit estimates. Transient increases in the tail temperature of the mouse to provocative motion are referred to as Δ tail vasodilatations (°C) and were computed by subtracting the tail temperature at time t = 0 minutes (rotation ON) from the max tail temperature measured during the first 10 mins of the rotation ($0 \leq t \leq 10$).

Pulse oximetry

A mouse Stat Jr X (Kent Scientific) was used to measure oxygen saturation (O2%) of mice (see Fig. 1B). The O_2 sensor was applied to the rear leg, and data were recorded following readout stabilization, defined as an unchanging recording over 5 seconds.

BAL harvest and tissue processing

Mice were euthanized with CO_2, and bronchoalveolar lavage BAL fluid was removed from the lungs; animals then underwent laparotomy and sternotomy with subsequent left and right ventricular cardiac perfusion with 20 mL total of PBS. The lungs were treated with 4% paraformaldehyde/PBS (vol/vol) for a minimum of 72 hours to ensure full viral inactivation. Tissues were taken out of the BSL3 facility, underwent dehydration with ethanol, and were later embedded in paraffin blocks for histological analysis.

Histopathology

For histological examination, mouse lungs were collected directly after euthanasia and placed in 10% neutral-buffered formalin for 72 hours, after which tissues were embedded in paraffin. Four-micrometer tissue sections were stained with hematoxylin for analysis. Immunohistochemistry and digital image analysis for SARS-CoV-2 nucleocapsids was performed as previously described (61). Briefly, 4-µm tissue sections were labeled with a rabbit IgG monoclonal antibody against the SARS-CoV-2 nucleocapsid protein (GeneTex; GTX635679) at a 1:5,000 dilution and processed using a Leica Bond Max automated IHC Stainer. Digital image analysis was performed using QuPath software v.0.2.3 (61–64).

Imaging

Histological specimens were visualized using a Zeiss Axioplan 2 microscope. Immunohistochemistry (IHC) and hematoxylin and eosin (HE)-stained slides for each specimen were photographed in sequential order. In Adobe Photoshop, all images were sized with a 2,080 × 2,080 pixel frame and cropped to a uniform resolution of 1,500 × 1,500 pixels. IHC images were further analyzed using Color Selection and Magic Wand tools where areas containing brown staining were manually selected and cut into a separate layer. All images were exported into JPEG format. For staining percentages, quantification was performed using ImageJ. Images were converted from RGB Color into an 8-bit grayscale and made binary to set an automated threshold. The area was then calculated with the Analyze Particles function. Circularity of staining was assessed using the Circularity parameter set to 0.9–1.0.

Quantification of lavage cytokines by ELISA

Immulon 4HBx plates (ThermoFisher Scientific, #3855) were coated with the IL-6 capture antibody (ThermoFisher Scientific, MP5-20F3) and left overnight at 4°C. Wells were washed five times with PBS + 0.05% Tween 20 and blocked with PBS + 5% dry milk solution (Bio-Rad, 1706404) for 1 hour at room temperature. Fifty microliters of the lavage sample or standard (R&D systems, 406 ML-005/CF) was added to the blocked wells for 2 hours at room temperature. Bound cytokines were detected using a biotinylated IL-6 detection antibody (ThermoFisher Scientific, MP5-32C11), streptavidin horseradish peroxidase (strep-HRP), and tetramethylbenzidine (TMB) (ThermoFisher Scientific, 34028). Wells were washed three times following the addition of the detection antibody and strep-HRP. Reactions were stopped with 2N H_2SO_4, and ODs were read at 450 nm. Cytokine concentrations for each sample were determined by plotting OD values on a standard curve using IL-6 recombinant protein. All testing was performed in triplicate.

Statistical analyses

Two-way mixed-effects (ME) models were used to assess % weight loss and core temperatures (°C) across the factors: (i) placebo vs olcegepant protection and (ii) dpi. Two-way ME models were also used to assess (i) viral infection vs pretest and (ii) placebo vs olcegepant protection for tail vasodilation responses at 3 dpi. The Bonferroni multiple comparisons test was the preferred *post-hoc* analysis method. X-intercept analyses of head recovery (mins) were conducted assuming a quadratic model, least squares regression fitting, and constraints where the x-intercept must be greater than x = 20 mins and the curve fit was approximated to x = 50 mins. Nested ne-way ANOVAs with Tukey's *post-hoc* test were used to analyze BAL IL-6 concentrations and H&E staining (positive SARS-CoV-2 cells per mm^2).

ACKNOWLEDGMENTS

This research is supported by a COVID-19 research supplement to NIH R01 DC017261 (to A.E.L. with sub-contract to H.C.A.).

We would also like to thank Dr. Ralph S. Baric (UNC) for the MA-10 SARS CoV-2 virus stock, the BSL3 facility and staff in the Center for Advanced Research Technologies at the

University of Rochester, and the A-BSL3 facility staff at Cornell University. We would also like to thank Shruti Aryal for assisting with data analysis.

AUTHOR AFFILIATIONS

[1]Departments of Biomedical Engineering, Neuroscience, Microbiology and Immunology, University of Rochester Medical Center, Rochester, New York, USA
[2]Department of Microbiology and Immunology, College of Veterinary Medicine, Cornell University, Ithaca, New York, USA
[3]Department of Population Medicine, College of Veterinary Medicine, Cornell University, Ithaca, New York, USA

AUTHOR ORCIDs

Shafaqat M. Rahman http://orcid.org/0000-0002-0877-1606
Raven M. Osborn http://orcid.org/0000-0002-6835-8856
Hector C. Aguilar http://orcid.org/0000-0001-6879-8360
Anne E. Luebke http://orcid.org/0000-0001-5651-0278

FUNDING

Funder	Grant(s)	Author(s)
HHS | National Institutes of Health (NIH)	R01 DC017261	Hector C. Aguilar Anne E. Luebke

ETHICS APPROVAL

Mouse studies were conducted in a BSL-3 laboratory and in accordance with protocols approved by the Institutional Animal Care and Use Committee at Cornell University (IACUC mouse protocol # 2017-0108 and BSL3 IBC # MUA-16371-1). All animal procedures were approved both by the University of Rochester's and Cornell University's IACUC committees and performed in accordance with NIH standards.

REFERENCES

1. Zhu N, Zhang D, Wang W, Li X, Yang B, Song J, Zhao X, Huang B, Shi W, Lu R, Niu P, Zhan F, Ma X, Wang D, Xu W, Wu G, Gao GF, Tan W, China Novel Coronavirus I, Research T. 2020. A novel coronavirus from patients with pneumonia in China, 2019. N Engl J Med 382:727–733. https://doi.org/10.1056/NEJMoa2001017
2. Liotta EM, Batra A, Clark JR, Shlobin NA, Hoffman SC, Orban ZS, Koralnik IJ. 2020. Frequent neurologic manifestations and encephalopathy-associated morbidity in COVID-19 patients. Ann Clin Transl Neurol 7:2221–2230. https://doi.org/10.1002/acn3.51210
3. Redd WD, Zhou JC, Hathorn KE, McCarty TR, Bazarbashi AN, Thompson CC, Shen L, Chan WW. 2020. Prevalence and characteristics of gastrointestinal symptoms in patients with severe acute respiratory syndrome coronavirus 2 infection in the United States: a multicenter cohort study. Gastroenterology 159:765–767. https://doi.org/10.1053/j.gastro.2020.04.045
4. Elbeltagi R, Al-Beltagi M, Saeed NK, Bediwy AS. 2023. COVID-19-induced gastrointestinal autonomic dysfunction: a systematic review. World J Clin Cases 11:5252–5272. https://doi.org/10.12998/wjcc.v11.i22.5252
5. Andrews PLR, Cai W, Rudd JA, Sanger GJ. 2021. COVID-19, nausea, and vomiting. J Gastroenterol Hepatol 36:646–656. https://doi.org/10.1111/jgh.15261
6. Bohn MK, Hall A, Sepiashvili L, Jung B, Steele S, Adeli K. 2020. Pathophysiology of COVID-19: mechanisms underlying disease severity and progression. Physiology (Bethesda) 35:288–301. https://doi.org/10.1152/physiol.00019.2020
7. Saniasiaya J, Kulasegarah J. 2021. Dizziness and COVID-19. Ear Nose Throat J 100:29–30. https://doi.org/10.1177/0145561320959573
8. Doyle MF. 2022. Central nervous system outcomes of COVID-19. Transl Res 241:41–51. https://doi.org/10.1016/j.trsl.2021.09.002
9. Bolay H, Karadas Ö, Oztürk B, Sonkaya R, Tasdelen B, Bulut TDS, Gülbahar Ö, Özge A, Baykan B. 2021. HMGB1, NLRP3, IL-6 and ACE2 levels are elevated in COVID-19 with headache: a window to the infection-related headache mechanism. J Headache Pain 22:94. https://doi.org/10.1186/s10194-021-01306-7
10. Goadsby PJ, Lipton RB, Ferrari MD. 2002. Migraine--current understanding and treatment. N Engl J Med 346:257–270. https://doi.org/10.1056/NEJMra010917
11. Lassen LH, Haderslev PA, Jacobsen VB, Iversen HK, Sperling B, Olesen J. 2002. CGRP may play a causative role in migraine. Cephalalgia 22:54–61. https://doi.org/10.1046/j.1468-2982.2002.00310.x
12. Tringali G, Navarra P. 2019. Anti-CGRP and anti-CGRP receptor monoclonal antibodies as antimigraine agents. Potential differences in safety profile postulated on a pathophysiological basis. Peptides 116:16–21. https://doi.org/10.1016/j.peptides.2019.04.012
13. Scuteri D, Adornetto A, Rombolà L, Naturale MD, Morrone LA, Bagetta G, Tonin P, Corasaniti MT. 2019. New trends in migraine pharmacology: targeting calcitonin gene-related peptide (CGRP) with monoclonal antibodies. Front Pharmacol 10:363. https://doi.org/10.3389/fphar.2019.00363
14. Assas BM, Miyan JA, Pennock JL. 2014. Cross-talk between neural and immune receptors provides a potential mechanism of homeostatic regulation in the gut mucosa. Mucosal Immunol 7:1283–1289. https://doi.org/10.1038/mi.2014.80

15. Assas BM, Pennock JI, Miyan JA. 2014. Calcitonin gene-related peptide is a key neurotransmitter in the neuro-immune axis. Front Neurosci 8:23. https://doi.org/10.3389/fnins.2014.00023
16. Channappanavar R, Perlman S. 2017. Pathogenic human coronavirus infections: causes and consequences of cytokine storm and immunopathology. Semin Immunopathol 39:529–539. https://doi.org/10.1007/s00281-017-0629-x
17. Aghagoli G, Gallo Marin B, Katchur NJ, Chaves-Sell F, Asaad WF, Murphy SA. 2021. Neurological involvement in COVID-19 and potential mechanisms: a review. Neurocrit Care 34:1062–1071. https://doi.org/10.1007/s12028-020-01049-4
18. Liu Y, Zhang C, Huang F, Yang Y, Wang F, Yuan J, Zhang Z, Qin Y, Li X, Zhao D, et al. 2020. Elevated plasma levels of selective cytokines in COVID-19 patients reflect viral load and lung injury. Natl Sci Rev 7:1003–1011. https://doi.org/10.1093/nsr/nwaa037
19. Carpenter KC, Yang J, Xu JJ. 2023. Animal models for the study of neurologic manifestations of COVID-19. Comp Med 73:91–103. https://doi.org/10.30802/AALAS-CM-22-000073
20. Robertson CE. 2020. Could CGRP antagonists be helpful in the fight against COVID-19? Headache 60:1450–1452. https://doi.org/10.1111/head.13853
21. Kuba K, Imai Y, Rao S, Gao H, Guo F, Guan B, Huan Y, Yang P, Zhang Y, Deng W, Bao L, Zhang B, Liu G, Wang Z, Chappell M, Liu Y, Zheng D, Leibbrandt A, Wada T, Slutsky AS, Liu D, Qin C, Jiang C, Penninger JM. 2005. A crucial role of angiotensin converting enzyme 2 (ACE2) in SARS coronavirus-induced lung injury. Nat Med 11:875–879. https://doi.org/10.1038/nm1267
22. Ziegler CGK, Allon SJ, Nyquist SK, Mbano IM, Miao VN, Tzouanas CN, Cao Y, Yousif AS, Bals J, Hauser BM, et al. 2020. SARS-CoV-2 receptor ACE2 is an interferon-stimulated gene in human airway epithelial cells and is detected in specific cell subsets across tissues. Cell 181:1016–1035. https://doi.org/10.1016/j.cell.2020.04.035
23. Dinnon KH, Leist SR, Schäfer A, Edwards CE, Martinez DR, Montgomery SA, West A, Yount BL, Hou YJ, Adams LE, Gully KL, Brown AJ, Huang E, Bryant MD, Choong IC, Glenn JS, Gralinski LE, Sheahan TP, Baric RS. 2020. A mouse-adapted model of SARS-CoV-2 to test COVID-19 countermeasures. Nature 586:560–566. https://doi.org/10.1038/s41586-020-2708-8
24. Dinnon KH, Leist SR, Schäfer A, Edwards CE, Martinez DR, Montgomery SA, West A, Yount BL, Hou YJ, Adams LE, Gully KL, Brown AJ, Huang E, Bryant MD, Choong IC, Glenn JS, Gralinski LE, Sheahan TP, Baric RS. 2021. Publisher Correction: a mouse-adapted model of SARS-CoV-2 to test COVID-19 countermeasures. Nature 590:E22. https://doi.org/10.1038/s41586-020-03107-5
25. Rahman SM, Luebke AE. 2024. Calcitonin gene-related peptide receptor antagonism reduces motion sickness indicators in mouse migraine models. Cephalalgia 44:3331024231223971. https://doi.org/10.1177/03331024231223971
26. Del Vecchio F, Nalivaiko E, Cerri M, Luppi M, Amici R. 2014. Provocative motion causes fall in brain temperature and affects sleep in rats. Exp Brain Res 232:2591–2599. https://doi.org/10.1007/s00221-014-3899-8
27. Mazloumi Gavgani A, Hodgson DM, Nalivaiko E. 2017. Effects of visual flow direction on signs and symptoms of cybersickness. PLoS One 12:e0182790. https://doi.org/10.1371/journal.pone.0182790
28. Ngampramuan S, Cerri M, Del Vecchio F, Corrigan JJ, Kamphee A, Dragic AS, Rudd JA, Romanovsky AA, Nalivaiko E. 2014. Thermoregulatory correlates of nausea in rats and musk shrews. Oncotarget 5:1565–1575. https://doi.org/10.18632/oncotarget.1732
29. Romano F, Caramia N, Straumann D, Nalivaiko E, Bertolini G. 2017. Cross-coupling vestibular stimulation: motion sickness and the vestibulo-sympathetic reflex. J Neurol 264:96–103. https://doi.org/10.1007/s00415-017-8496-x
30. Tu L, Poppi L, Rudd J, Cresswell ET, Smith DW, Brichta A, Nalivaiko E. 2017. Alpha-9 nicotinic acetylcholine receptors mediate hypothermic responses elicited by provocative motion in mice. Physiol Behav 174:114–119. https://doi.org/10.1016/j.physbeh.2017.03.012
31. Doods H, Hallermayer G, Wu D, Entzeroth M, Rudolf K, Engel W, Eberlein W. 2000. Pharmacological profile of BIBN4096BS, the first selective small molecule CGRP antagonist. Br J Pharmacol 129:420–423. https://doi.org/10.1038/sj.bjp.0703110
32. Mallee JJ, Salvatore CA, LeBourdelles B, Oliver KR, Longmore J, Koblan KS, Kane SA. 2002. Receptor activity-modifying protein 1 determines the species selectivity of non-peptide CGRP receptor antagonists. J Biol Chem 277:14294–14298. https://doi.org/10.1074/jbc.M109661200
33. Shafaqat MR, Anne EL. 2023. Calcitonin gene-related peptide (CGRP) receptor antagonism reduces motion sickness indicators in mouse migraine models. bioRxiv. https://doi.org/10.1101/2022.06.03.494762:2022.06.03.494762
34. Han D. 2019. Association of serum levels of calcitonin gene-related peptide and cytokines during migraine attacks. Ann Indian Acad Neurol 22:277–281. https://doi.org/10.4103/aian.AIAN_371_18
35. Aedo-Sánchez C, Gutiérrez G, Aguilar-Vidal E. 2024. COVID-19 and vestibular symptoms and assessment: a review. Audiol Neurootol 29:81–87. https://doi.org/10.1159/000533448
36. Jeong M, Ocwieja KE, Han D, Wackym PA, Zhang Y, Brown A, Moncada C, Vambutas A, Kanne T, Crain R, Siegel N, Leger V, Santos F, Welling DB, Gehrke L, Stankovic KM. 2021. Direct SARS-CoV-2 infection of the human inner ear may underlie COVID-19-associated audiovestibular dysfunction. Commun Med (Lond) 1:44. https://doi.org/10.1038/s43856-021-00044-w
37. Abobaker A, Darrat M. 2021. Letter to the editor from Abobaker and Darrat: "circulating levels of calcitonin gene-related peptide are lower in COVID-19 patients". J Endocr Soc 5:bvab052. https://doi.org/10.1210/jendso/bvab052
38. Ochoa-Callejero L, García-Sanmartín J, Villoslada-Blanco P, Íñiguez M, Pérez-Matute P, Pujadas E, Brody R, Oteo JA, Martínez A. 2021. Response to letter to the editor from Abobaker and Darrat: "circulating levels of calcitonin gene-related peptide are lower in COVID-19 patients". J Endocr Soc 5:bvab053. https://doi.org/10.1210/jendso/bvab053
39. Rizzi M, Tonello S, Morani F, Rizzi E, Casciaro GF, Matino E, Costanzo M, Zecca E, Croce A, Pedrinelli A, Vassia V, Landi R, Mallela VR, D'Onghia D, Minisini R, Bellan M, Castello LM, Gavelli F, Avanzi GC, Patrucco F, Pirisi M, Colangelo D, Sainaghi PP. 2022. CGRP plasma levels correlate with the clinical evolution and prognosis of hospitalized acute COVID-19 patients. Viruses 14:2123. https://doi.org/10.3390/v14102123
40. Rothaug M, Becker-Pauly C, Rose-John S. 2016. The role of interleukin-6 signaling in nervous tissue. Biochim Biophys Acta 1863:1218–1227. https://doi.org/10.1016/j.bbamcr.2016.03.018
41. Pattanaik A, Bhandarkar B S, Lodha L, Marate S. 2023. SARS-CoV-2 and the nervous system: current perspectives. Arch Virol 168:171. https://doi.org/10.1007/s00705-023-05801-x
42. Barton LM, Duval EJ, Stroberg E, Ghosh S, Mukhopadhyay S. 2020. COVID-19 autopsies, Oklahoma, USA. Am J Clin Pathol 153:725–733. https://doi.org/10.1093/ajcp/aqaa062
43. Deng T, Yang L, Zheng Z, Li Y, Ren W, Wu C, Guo L. 2017. Calcitonin gene-related peptide induces IL-6 expression in RAW264.7 macrophages mediated by mmu_circRNA_007893. Mol Med Rep 16:9367–9374. https://doi.org/10.3892/mmr.2017.7779
44. Ebbinghaus M, Segond von Banchet G, Massier J, Gajda M, Bräuer R, Kress M, Schaible H-G. 2015. Interleukin-6-dependent influence of nociceptive sensory neurons on antigen-induced arthritis. Arthritis Res Ther 17:334. https://doi.org/10.1186/s13075-015-0858-0
45. Leo S, Straetemans R, D'Hooge R, Meert T. 2008. Differences in nociceptive behavioral performance between C57BL/6J, 129S6/SvEv, B6 129 F1 and NMRI mice. Behav Brain Res 190:233–242. https://doi.org/10.1016/j.bbr.2008.03.001
46. Mogil JS, Wilson SG, Bon K, Lee SE, Chung K, Raber P, Pieper JO, Hain HS, Belknap JK, Hubert L, Elmer GI, Chung JM, Devor M. 1999. Heritability of nociception I: responses of 11 inbred mouse strains on 12 measures of nociception. Pain 80:67–82. https://doi.org/10.1016/s0304--3959(98)00197-3
47. Zhou YQ, Liu Z, Liu ZH, Chen SP, Li M, Shahveranov A, Ye DW, Tian YK. 2016. Interleukin-6: an emerging regulator of pathological pain. J Neuroinflammation 13:141. https://doi.org/10.1186/s12974-016-0607-6
48. Caronna E, José Gallardo V, Alpuente A, Torres-Ferrus M, Sánchez-Mateo NM, Viguera-Romero J, López-Veloso AC, López-Bravo A, Gago-Veiga AB, Irimia Sieira P, Porta-Etessam J, Santos-Lasaosa S, Pozo-Rosich P, Spanish CGRP-COVID Study Group. 2021. Safety of anti-CGRP monoclonal antibodies in patients with migraine during the COVID-19 pandemic: present and future implications. Neurologia (Engl Ed) 36:611–617. https://doi.org/10.1016/j.nrl.2021.03.003
49. Grassini A, Marcinnò A, Roveta F, Gallo E, Cermelli A, Boschi S, Rubino E, Rainero I. 2021. Impact of COVID-19 on chronic migraine treated with

erenumab: a case report. Neurol Sci 42:3079–3081. https://doi.org/10.1007/s10072-021-05329-5
50. Özkan E, Celebi Ö, Keskin Ö, Gursoy A, Gürsoy-Özdemir Y. 2022. Is persistent post-COVID headache associated with protein-protein interactions between antibodies against viral spike protein and CGRP receptor?: a case report. Front Pain Res (Lausanne) 3:858709. https://doi.org/10.3389/fpain.2022.858709
51. Kaiser EA, Kuburas A, Recober A, Russo AF. 2012. Modulation of CGRP-induced light aversion in wild-type mice by a 5-HT(1B/D) agonist. J Neurosci 32:15439–15449. https://doi.org/10.1523/JNEUROSCI.3265-12.2012
52. Mason BN, Kaiser EA, Kuburas A, Loomis M-C, Latham JA, Garcia-Martinez LF, Russo AF. 2017. Induction of migraine-like photophobic behavior in mice by both peripheral and central CGRP mechanisms. J Neurosci 37:204–216. https://doi.org/10.1523/JNEUROSCI.2967-16.2016
53. Recober A, Kuburas A, Zhang Z, Wemmie JA, Anderson MG, Russo AF. 2009. Role of calcitonin gene-related peptide in light-aversive behavior: implications for migraine. J Neurosci 29:8798–8804. https://doi.org/10.1523/JNEUROSCI.1727-09.2009
54. Russo AF. 2015. CGRP as a neuropeptide in migraine: lessons from mice. Br J Clin Pharmacol 80:403–414. https://doi.org/10.1111/bcp.12686
55. Wang M, Mason BN, Sowers LP, Kuburas A, Rea BJ, Russo AF. 2021. Investigating migraine-like behavior using light aversion in mice. J Vis Exp 174. https://doi.org/10.3791/62839
56. Littlefield KM, Watson RO, Schneider JM, Neff CP, Yamada E, Zhang M, Campbell TB, Falta MT, Jolley SE, Fontenot AP, Palmer BE. 2022. SARS-CoV-2-specific T cells associate with inflammation and reduced lung function in pulmonary post-acute sequalae of SARS-CoV-2. PLoS Pathog 18:e1010359. https://doi.org/10.1371/journal.ppat.1010359
57. Dinnon KH, Leist SR, Okuda K, Dang H, Fritch EJ, Gully KL, De la Cruz G, Evangelista MD, Asakura T, Gilmore RC, et al. 2022. A model of persistent post SARS-CoV-2 induced lung disease for target identification and testing of therapeutic strategies. bioRxiv:2022.02.15.480515. https://doi.org/10.1101/2022.02.15.480515
58. Jansen EB, Orvold SN, Swan CL, Yourkowski A, Thivierge BM, Francis ME, Ge A, Rioux M, Darbellay J, Howland JG, Kelvin AA. 2022. After the virus has cleared-can preclinical models be employed for long COVID research? PLoS Pathog 18:e1010741. https://doi.org/10.1371/journal.ppat.1010741
59. Nalivaiko E. 2018. Thermoregulation and nausea. Handb Clin Neurol 156:445–456. https://doi.org/10.1016/B978-0-444-63912-7.00027-8
60. Rudd JA, Nalivaiko E, Matsuki N, Wan C, Andrews PL. 2015. The involvement of TRPV1 in emesis and anti-emesis. Temperature (Austin) 2:258–276. https://doi.org/10.1080/23328940.2015.1043042
61. Shapira T, Monreal IA, Dion SP, Buchholz DW, Imbiakha B, Olmstead AD, Jager M, Désilets A, Gao G, Martins M, et al. 2022. A TMPRSS2 inhibitor acts as a pan-SARS-CoV-2 prophylactic and therapeutic. Nature 605:340–348. https://doi.org/10.1038/s41586-022-04661-w
62. Achanta R, Shaji A, Smith K, Lucchi A, Fua P, Süsstrunk S. 2012. SLIC superpixels compared to state-of-the-art superpixel methods. IEEE Trans Pattern Anal Mach Intell 34:2274–2282. https://doi.org/10.1109/TPAMI.2012.120
63. Bankhead P, Loughrey MB, Fernández JA, Dombrowski Y, McArt DG, Dunne PD, McQuaid S, Gray RT, Murray LJ, Coleman HG, James JA, Salto-Tellez M, Hamilton PW. 2017. QuPath: open source software for digital pathology image analysis. Sci Rep 7:16878. https://doi.org/10.1038/s41598-017-17204-5
64. Shapira T, Monreal IA, Dion SP, Jager M, Désilets A, Olmstead AD, Vandal T, Buchholz DW, Imbiakha B, Gao G, Chin A, Rees WD, Steiner T, Nabi IR, Marsault E, Sahler J, August A, Van de Walle G, Whittaker GR, Boudreault P-L, Aguilar HC, Leduc R, Jean F. 2021. A novel highly potent inhibitor of TMPRSS2-like proteases blocks SARS-CoV-2 variants of concern and is broadly protective against infection and mortality in mice. bioRxiv:2021.05.03.442520. https://doi.org/10.1101/2021.05.03.442520